Proceedings of the 2001 IEEE/RSJ
International Conference on Intelligent Robots and Systems
Maui, Hawaii, USA, Oct. 29 – Nov. 03, 2001

# Design and Analysis of a Spatial 3-DOF Micromanipulator for Tele-operation

**Goo Bong Chung*, Byung-Ju Yi*, Il Hong Suh*, Whee Kuk Kim**, Wan Kyun Chung*****

*School of Electrical Engineering and Computer Science, Hanyang Univ., KOREA
**School of Control and Instrumentation, Korea Univ., KOREA
***Department of Mechanical engineering, POSTECH, KOREA
E-mail: bj@hanyang.ac.kr

**Abstract**

*In this paper, we propose and develop a spatial 3-DOF tele-micromanipulator for precise position control of micro-objects. Typical feature of this device is a one-moduled flexure hinge that consists of a revolute joint and a spherical joint. Based on preliminary kinematic analysis and stiffness modeling of the system, optimal design and actuator sizing for the device are performed. Furthermore, FEM analysis and resonant frequency analysis are executed to validate the results of analytic design process. The designed device was successfully implemented to tele-micromanipulation system.*

## 1. Introduction

In days past, a technique to manipulate microscopic objects was understood difficult, but it is progressing together with the advancement of an electron microscope, signal processing techniques, and precision mechanisms. The necessity of handling smaller and smaller objects is on the increase due to the advent of applications such as assembling micromachines, micro-surgery, and manipulating bio-cells. In order to apply those micro mechanisms to various applications, functionality of multi degree-of-freedom is essential. Recently, many micro-tele devices have been reported[1-5]. Such devices should ensure position accuracy in the order of sub-micron meter. However, current state of art in manufacturing process does not fully support this requirement. Also, calibration process is very crucial after the device is fabricated. Thus, in order to alleviate the loss of positioning accuracy, we propose and develop a new 3-DOF micromanipulator with high precision. Typical feature of this device is one-moduled serial chain with a monolithic configuration that consists of a revolute joint and a spherical joint as shown in Fig. 1. This configuration is able to minimize the additional backlash or inaccuracy caused by connecting two different modules. Furthermore, the device is designed in such a way to obviate the vibration effects observed in the microscopic world by taking into account the resonant frequencies of its structure in the design process. The organization of this paper is as follows; Section 2 deals with the kinematics of the proposed 3-DOF micromanipulator. Based on the kinematic model, optimal design for the 3-DOF micromanipulator is performed in section 3. The actuator size and hinge parameters are determined in section 4. In section 5, FEM analysis and resonant frequency analysis are performed to validate the results of our analytic design process. The designed device was successfully implemented to tele-micromanipulation system having positioning accuracy of sub-microns. Finally, section 6 draws conclusion.

## 2. Kinematics

As shown in Fig. 2, the proposed micromanipulator is a parallel-type mechanism composed of three serial chains. Each chain consists of a spherical joint, a revolute joint, and a prismatic joint located at the base.

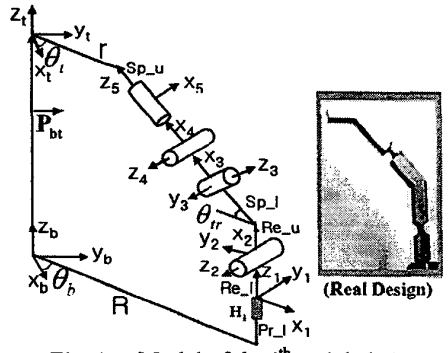


Fig. 1. Model of the $i^{th}$ serial chain

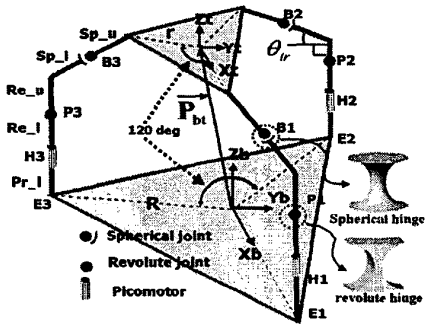


Fig. 2. 3-DOF micromanipulator

0-7803-6612-3/01/$10.00©2001 IEEE

The spherical and the revolute joints are fabricated as an one-moduled flexure hinge. The flexure hinge behaves like mechanical joints by their compliances. The detailed description of each serial chain is shown in Fig. 2. R and r are the radius of the lower plate and the upper plate, respectively. The prismatic joint denotes the displacement ($H_i$) of piezo-actuator. The second joint denotes a revolute flexure hinge. And the spherical flexure hinge is modeled by 3rd, 4th and 5th joint. $\overrightarrow{P_{bt}}$ is a position vector, which locates the center of the upper plate relative to the global coordinate located at the lower plate.

The transformation of the local coordinate attached to the upper plate with respect to the global coordinate can be described by

$$T_t^b \triangleq \begin{bmatrix} n_1 & o_1 & a_1 & x_c \\ n_2 & o_2 & a_2 & y_c \\ n_3 & o_3 & a_3 & z_c \\ 0 & 0 & 0 & 1 \end{bmatrix}. \quad (1)$$

The output vector $\underline{u}$ of the proposed mechanism is composed of the positions, $x_c$, $y_c$, $z_c$ and x-y-z Euler angles, $\alpha$, $\beta$, $\gamma$. Since the number of mobility of this system is three, the independent output vector $\underline{u}_{ind}$ is decided as $\alpha$, $\beta$, $z_c$ and the remaining components are treated as the elements of the dependent output vector $\underline{u}_{dep}$. The input vector ${}^i\underline{\phi}$ of the i[th] serial chain is defined as

$${}^i\underline{\phi} = [H_i, {}^i\theta_2, {}^i\theta_3, {}^i\theta_4, {}^i\theta_5]^T \triangleq [{}^i\phi_1, {}^i\phi_2, {}^i\phi_3, {}^i\phi_4, {}^i\phi_5]^T. \quad (2)$$

### 2.1 Inverse Kinematics

The inverse kinematics calculates the input vector ${}^i\underline{\phi}$ of each chain for a given independent output vector $\underline{u}_{ind} = (\alpha \ \ \beta \ \ z_c)^T$. $\underline{P}_i$ denote the position vector of the point $P_i$ in the i[th] chain with respect to the global coordinates.

Furthermore, the position vector $\underline{b}_i$ of the point $B_i$ with respect to the local coordinate fixed on the upper plate is described as

$$\underline{b}_1 = [b_{1x}, \ 0, \ -b_{1z}]^T,$$

$$\underline{b}_2 = [-\frac{1}{2}b_{1x}, \ \frac{\sqrt{3}}{2}b_{1x}, \ -b_{1z}]^T,$$

and

$$\underline{b}_3 = [-\frac{1}{2}b_{1x}, \ -\frac{\sqrt{3}}{2}b_{1x}, \ -b_{1z}]^T, \quad (3)$$

where $b_{1x} = r + Sp\_u\cos\theta_{tr}$ and $b_{1z} = Sp\_u\sin\theta_{tr}$.

The $\underline{b}_i$ can be described with respect to the global reference coordinates as follows

$$\begin{bmatrix} \underline{B}_i \\ 1 \end{bmatrix} = \begin{bmatrix} T_t^b \end{bmatrix} \begin{bmatrix} \underline{b}_i \\ 1 \end{bmatrix}. \quad (i = 1,2,3) \quad (4)$$

By using Eq. (4), the position vectors of the point $B_i$ written in the global coordinates can be obtained.

As the links $\overline{B_1P_1}$, $\overline{B_2P_2}$ and $\overline{B_3P_3}$ are constrained by the revolute joints to move in the planes $Y = 0$, $Y = -\sqrt{3}X$, and $Y = \sqrt{3}X$, respectively. The constraint equations imposed by the revolute joints are

$$y_c = -n_2 b_{1x} + a_2 b_{1z}, \quad (5)$$

$$n_2 = o_1, \quad (6)$$

and

$$x_c = -\frac{1}{2}(o_2 b_{1x} - n_1 b_{1x} - 2a_1 b_{1z}). \quad (7)$$

Then, by using x-y-z Euler angles, the elements of the Eq. (1) can be expressed as

$$\begin{aligned} n_1 &= \cos\beta\cos\gamma \\ n_2 &= \sin\alpha\sin\beta\cos\gamma + \cos\alpha\sin\gamma \\ n_3 &= -\cos\alpha\sin\beta\cos\gamma + \sin\alpha\sin\gamma \\ o_1 &= -\cos\beta\sin\gamma \\ o_2 &= -\sin\alpha\sin\beta\sin\gamma + \cos\alpha\cos\gamma \\ o_3 &= \cos\alpha\sin\beta\sin\gamma + \sin\alpha\cos\gamma \\ a_1 &= \sin\beta \\ a_2 &= -\sin\alpha\cos\beta \\ a_3 &= \cos\alpha\cos\beta \end{aligned} \quad (8)$$

From Eq. (6) through Eq. (8), Euler angle $\gamma$ about z-axis of global coordinates is obtained as

$$\gamma = \arctan(-\frac{\sin\alpha\sin\beta}{\cos\alpha + \cos\beta}). \quad (9)$$

Substituting $\gamma$ and the given $\alpha$, $\beta$ into Eq. (8), all the elements of $T_t^b$ are obtained, and then, $x_c$ and $y_c$ are calculated from Eq. (5) and Eq. (7). Therefore, $B_i$ is obtained by Eq. (5). The length between the point $B_i$ and $P_i$ are

$$\overline{B_iP_i} = \{(B_{ix} - P_{ix})^2 + (B_{iy} - P_{iy})^2 + (B_{iz} - P_{iz})^2\}^{0.5}, \quad (10)$$

where $B_{ix}$, $B_{iy}$, $B_{iz}$, $P_{ix}$, $P_{iy}$, and $P_{iz}$ denote the elements of the position vectors of the point $B_i$ and $P_i$ with respect to global coordinate. Therefore, the active joint variable $H_i$ is obtained as

$$H_i = B_{iz} - \mathrm{Pr}\_l - \mathrm{Re}\_l - (\overline{B_iP_i}^2 - (B_{ix} - P_{ix})^2 - (B_{iy} - P_{iy})^2)^{0.5}. \quad (11)$$

A revolute joint variable ${}^i\theta_2$ of the $i^{th}$ chain is obtained geometrically from Fig. 3 as follows

$${}^i\theta_2 = \pi/2 - {}^i\theta_d - {}^i\theta. \quad (12)$$

Also, the spherical joint variables of the $i^{th}$ chain, ${}^i\theta_3$, ${}^i\theta_4$, and ${}^i\theta_5$ are obtained from

$$ {}^{i}[T_1^2]\,{}^{i}[T_h^1]\,[T_r^h]\,{}^{i}[T_5^r] = {}^{i}[T_3^2]\,{}^{i}[T_4^3]\,{}^{i}[T_5^4], \quad (13) $$

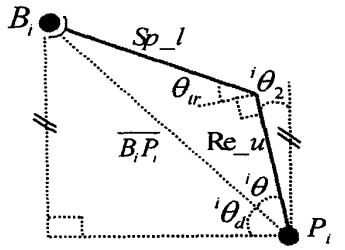

Fig. 3. Geometric solution of ${}^{i}\theta_2$

where ${}^{i}[T_k^j]$ is a matrix which transforms the $k^{th}$ coordinate into the $j^{th}$ coordinate of the $i^{th}$ chain. The left-side of Eq. (13) is known and the right-side is the function of ${}^{i}\theta_3$, ${}^{i}\theta_4$, and ${}^{i}\theta_5$. Let the left term be defined as

$$ {}^{i}[T_1^2]\,{}^{i}[T_h^1]\,[T_r^h]\,{}^{i}[T_5^r] \triangleq \begin{bmatrix} e_1 & f_1 & g_1 & i_1 \\ e_2 & f_2 & g_2 & i_2 \\ e_3 & f_3 & g_3 & i_3 \\ 0 & 0 & 0 & 1 \end{bmatrix}. \quad (14) $$

By using Eq. (13) and Eq. (14), the spherical joint variables are obtained as

$$ {}^{i}\theta_3 = \tan^{-1}\left(\frac{g_3}{g_1\cos\theta_{tr} + g_2\sin\theta_{tr}}\right), \quad (15) $$

$$ {}^{i}\theta_4 = A\tan 2(g_2\cos\theta_{tr} - g_1\sin\theta_{tr}, \frac{g_1\cos\theta_{tr} + g_2\sin\theta_{tr}}{\cos{}^{i}\theta_3}), \quad (16) $$

and

$$ {}^{i}\theta_5 = \tan^{-1}\left(\frac{e_2 - e_1}{f_2 - f_1}\right). \quad (17) $$

### 2.2 First-order Kinematics

The velocity vector of the end-effector for the $i^{th}$ chain can be expressed directly in terms of the $i^{th}$ joint velocity vector as

$$ \underline{\dot{u}} = [{}_iG_\phi^u]\,{}^{i}\underline{\dot{\phi}}, \quad (18) $$

where the output velocity vector is denoted as

$$ \underline{\dot{u}} = \begin{bmatrix} \underline{\dot{P}} \\ \underline{\omega}_{Eul} \end{bmatrix} \quad (19) $$

and $\underline{\dot{P}}$ and $\underline{\omega}_{Eul}$ is defined as follows, respectively.

$$ \underline{\dot{P}} \triangleq [\dot{x}_c \quad \dot{y}_c \quad \dot{z}_c]^T = [{}_iG_\phi^P]\,{}^{i}\underline{\dot{\phi}}, \quad (20) $$

$$ \underline{\omega}_{Eul} \triangleq [\dot{\alpha} \quad \dot{\beta} \quad \dot{\gamma}]^T = [{}_iG_\phi^{Eul}]\,{}^{i}\underline{\dot{\phi}} = [G_{Fix}^{Eul}][{}_iG_\phi^{Fix}]\,{}^{i}\underline{\dot{\phi}}, \quad (21) $$

where $[{}_iG_\phi^P]$, $[G_{Fix}^{Eul}]$, and $[{}_iG_\phi^{Fix}]$ are given as, respectively

$$ [{}_iG_\phi^P] = [{}^{i}\underline{s}_1 \; {}^{i}\underline{s}_3 \times ({}^{i}\underline{P} - {}^{i}\underline{R}_2) \; {}^{i}\underline{s}_3 \times ({}^{i}\underline{P} - {}^{i}\underline{R}_3) \; {}^{i}\underline{s}_4 \times ({}^{i}\underline{P} - {}^{i}\underline{R}_4) \; {}^{i}\underline{s}_5 \times ({}^{i}\underline{P} - {}^{i}\underline{R}_5)], \quad (22) $$

$$ [G_{Fix}^{Eul}] = [G_{Eul}^{Fix}]^{-1}, \quad (23) $$

$$ [G_{Eul}^{Fix}] = \begin{bmatrix} 1 & 0 & \sin\beta \\ 0 & \cos\alpha & -\sin\alpha\cos\beta \\ 0 & \sin\alpha & \cos\alpha\cos\beta \end{bmatrix}, \quad (24) $$

and

$$ [{}_iG_\phi^{Fix}] = [\underline{0}_{(3\times1)} \; {}^{i}\underline{s}_2 \; {}^{i}\underline{s}_3 \; {}^{i}\underline{s}_4 \; {}^{i}\underline{s}_5]. \quad (25) $$

The vector ${}^{i}\underline{s}_j$ of Eq. (22) and Eq. (25) indicates the z-axis of the $j^{th}$ coordinate of the $i^{th}$ chain with respect to the global coordinate, and $\underline{P}$ denotes the position vector of the origin of the upper plate coordinate with respect to the global coordinate. Also, ${}^{i}\underline{R}_j$ means the position vector of the origin of the $j^{th}$ coordinate with respect to the global coordinate[6]. In Eq. (24), $[G_{Eul}^{Fix}]$ is a Jacobian relating to the Euler rate vector and the angular velocity vector with respect to the global coordinates[7]. So, Jacobian, $[{}_iG_\phi^u]$ of Eq. (18) is expressed as follows

$$ [{}_iG_\phi^u] = \begin{bmatrix} [{}_iG_\phi^P] \\ [{}_iG_\phi^{Eul}] \end{bmatrix}. \quad (26) $$

Since the three sub-chains have the same operational velocity at the upper plate, two loop constraint equations exist. By manipulation of these two loop constraint equations, a relation between the passive(dependent) joint velocity and the active(independent) joint velocity is obtained as below [6]

$$ \underline{\dot{\phi}}_p = [G_a^p]\,\underline{\dot{\phi}}_a, \quad (27) $$

In Eq. (27), the active joint vector, $\underline{\phi}_a$ and the passive joint vector, $\underline{\phi}_p$ is described as, respectively

$$ \underline{\phi}_a = [h_1, h_2, h_3]^T, \quad (28) $$

$$ \underline{\phi}_p = [{}^{1}\phi_2 \; {}^{1}\phi_3 \; {}^{1}\phi_4 \; {}^{1}\phi_5 \; {}^{2}\phi_2 \; {}^{2}\phi_3 \; {}^{2}\phi_4 \; {}^{2}\phi_5 \; {}^{3}\phi_2 \; {}^{3}\phi_3 \; {}^{3}\phi_4 \; {}^{3}\phi_5]^T. \quad (29) $$

Now, the joint velocity vector of the 1st chain can be described in terms of the independent joint variables:

$$ {}^{1}\underline{\dot{\phi}} = [{}_1G_a^\phi]\,\underline{\dot{\phi}}_a, \quad (30) $$

where

$$ [{}_1G_a^\phi] = \begin{bmatrix} 1 & & & \\ 0 & [G_a^p]_{1:}^T & [G_a^p]_{2:}^T & [G_a^p]_{3:}^T \; [G_a^p]_{4:}^T \\ 0 & & & \end{bmatrix}^T \quad (31) $$

and $[G_a^p]_{j:}$ denotes the $j^{th}$ row of $[G_a^p]$.

Substituting Eq. (30) into Eq. (18) results in the output velocity vector, given by

$$ \underline{\dot{u}} = [G_a^u]\,\underline{\dot{\phi}}_a, \; [G_a^u] = [{}_1G_\phi^u][{}_1G_a^\phi]. \quad (32) $$

Consequently, the relationship between independent output velocity and independent input velocity vector is selected from Eq. (32). We have

$$ \underline{\dot{u}}_{ind} = [\dot{\alpha}, \dot{\beta}, \dot{z}_c]^T = [G_a^{u_{ind}}]\,\underline{\dot{\phi}}_a, \quad (33) $$

where $[G_a^{u_{ind}}]$ is obtained by selecting three rows from $[G_a^u]$, corresponding the independent output components.

## 3. Optimal Design

### 3.1 Kinematic Isotropic Index

The Kinematic Isotropic Index is defined as

$$\sigma_I = \frac{\sigma_{\min}([G_a^{u_{ind}}])}{\sigma_{\max}([G_a^{u_{ind}}])}, \quad (34)$$

where $\sigma_{\min}$ and $\sigma_{\max}$ denote the minimum and the maximum singular values of $[G_a^{u_{ind}}]$, respectively. When $\sigma_I$ approaches unity, the end-effector can generate uniform velocity in all directions. Also, the global kinematic isotropic index is defined as

$$\Sigma_I = \frac{\int_v \sigma_I dV}{\int_v dV} \quad (35)$$

which represents the average of the kinematic isotropic index over the whole workspace. The greater $\Sigma_I$ is, the better isotropy the mechanism has over the workspace. Therefore, $\Sigma_I$ should be maximized.

### 3.2 Design Parameters

Design parameters for the proposed mechanism are the radius R of the lower plate, the crooked angle $\theta_{tr}$ between the revolute hinge and the spherical hinge, and the link lengths (Sp_u, Sp_l, and Re_u). We performed a kinematic optimization in such a way to maximize the global kinematic isotropic index $\Sigma_I$. Ranges of those design parameters and workspace are described in Table 1. Table 2 denotes optimal design parameters resulting from the optimization.

Table 1. Kinematic constraints (unit: $mm$, Deg.)

| Workspace | | | | | |
|---|---|---|---|---|---|
| $\alpha$ | | $\beta$ | | $z_t$ | |
| Max. | Min. | Max. | Min. | Max. | Min. |
| 3 | -3 | 3 | -3 | 70 | 45 |

| Design parameter | | | | | | | | | |
|---|---|---|---|---|---|---|---|---|---|
| R | | $\theta_{tr}$ | | $Sp\_l$ | | $Sp\_u$ | | Re_u | |
| Max. | Min. | Max. | Min. | Max. | Min. | Max. | Min. | Max. | Min. |
| 17 | 40 | 85 | 5 | 20 | 5 | 20 | 5 | 20 | 5 |

Table 2. Result of optimal design (unit: $mm$, Deg.)

| Design parameter | | | | |
|---|---|---|---|---|
| R | $\theta_{tr}$ | $Sp\_l$ | $Sp\_u$ | Re_u |
| 34.9 | 45 | 16.27 | 11.87 | 11.88 |

## 4. Actuator Sizing

In this section, we determine the actuator size required for the motion range of the given workspace. To cope with this problem, a relationship between actuator torque and the stiffness models of joints should be considered. By using the principle of virtual work, the relationship between the torque vector of active joints and passive joints are obtained as follows

$$\underline{\tau}_a^T \dot{\underline{\phi}}_a = \underline{\tau}_p^T \dot{\underline{\phi}}_p. \quad (36)$$

Substituting Eq. (27) into Eq. (36), an effective joint torque vector referenced to independent joint coordinate is described as

$$\underline{\tau}_a = [G_a^p]^T \underline{\tau}_p, \quad (37)$$

and the torque vector( $\tau_p$ ) at the passive joints is denoted as

$$\underline{\tau}_p = [K_{pp}]\delta\underline{\phi}_p, \quad (38)$$

where $[K_{pp}]$ is the stiffness matrix of passive joints(i.e., flexure hinges). A method to calculate the stiffnesses of the spherical and revolute hinges is well expressed in [8] and [9]. $\delta\underline{\phi}_p$ denotes the infinitesimal displacement of the flexure hinges of the system. Substituting $\underline{\tau}_p$ into Eq. (37) yields

$$\underline{\tau}_a = [G_a^p]^T [K_{pp}]\delta\underline{\phi}_p \quad (39)$$

which relates the actuator torque to the motion of the micromanipulator. It is shown that the internal Jacobian and the stiffnesses of flexure hinges are necessary as a mapping relation. Once the range of workspace and the stiffnesses of flexure hinges are given, the range of $\delta\underline{\phi}_p$ and the actuator size can be obtained from Eq. (27), (32), and (39), respectively. Reverse process which decides the stiffness of mechanical hinges for a given actuator size can be also performed. The stiffness of the flexure hinges is the function of the radius R, the minimum thickness t, and the width b of hinge. The calculated actuator torque and hinge parameters are denoted in Table 3.

Table 3. Actuator torque and hinge parameters

| Actuator torque | Revolute hinge | | | Spherical hinge | |
|---|---|---|---|---|---|
| | R | t | B | R | t |
| MAX. 22N | 1.65mm | 0.7mm | 4.0mm | 1.5mm | 1.0mm |

## 5. Analysis of the Developed 3-DOF Mechanism

### 5.1. Forward Kinematics

In general, the forward kinematic solution of parallel manipulators is not unique, but multiple. However, we can employ the infinitesimal kinematics of the device as a substitute of forward kinematic solution. A modified form of Eq. (33) is given by

$$\delta\underline{u}_{ind} = [G_a^{u_{ind}}]\delta\underline{\phi}_a. \quad (40)$$

Initially, FEM(Finite Element Method) is employed to obtain forward kinematic solution. Fig. 4 (a) shows the result of FEM when one of the actuators moves 100 $\mu m$ in the z-direction and Fig. 4 (b) shows the case when two of the three actuators move 172.72 $\mu m$ and 172.24 $\mu m$, respectively. FEM provides us with the joint information as well as the forward solution. Then, the joint

information resulting from FEM is employed in Eq. (40) to obtain a forward kinematic solution in an analytic manner.

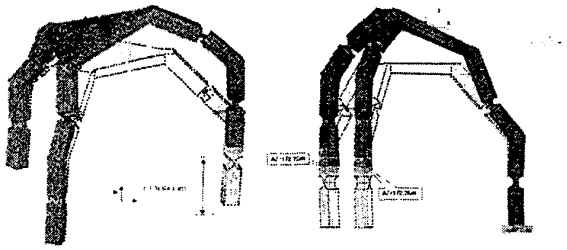

(a) Motion of one actuator (b) Motion of two actuators

Fig. 4. FEM analysis

As shown in Table 4, two simulation results are almost identical to the analytic solution. Therefore, FEM analysis is accepted as a useful means of estimating forward kinematic solution of the given tele-micromanipulators.

Table 4. Simulation results (unit: $\mu m$, Deg.)

| Actuated actuator number | | | 1 | 2 |
|---|---|---|---|---|
| Kinematics using FEM | Input | $h_1$ | 100.64 | 0 |
| | | $h_2$ | 0 | 172.72 |
| | | $h_3$ | 0 | 172.24 |
| | Output | $\alpha$ | About 0.00017 | About -0.0002653 |
| | | $\beta$ | About -0.1469 | About 0.2374 |
| | | $z_c$ | About 35.5 | About 100 |
| Kinematics using analytic method | Input | $\alpha$ | 0.00017 | -0.0002653 |
| | | $\beta$ | -0.1469 | 0.2374 |
| | | $z_c$ | 35.5 | 100 |
| | Output | $h_1$ | 104 | -9 |
| | | $h_2$ | 2 | 156 |
| | | $h_3$ | 2 | 156 |

### 5.2. Resonant Frequency Analysis

Since precision mechanisms are greatly influenced by the vibration effects in the microscopic world, those effects should be carefully analyzed. Thus, the structural resonant frequency of the micromanipulator should be first examined. Then, the system should be controlled in a frequency band not to excite vibration of the system. In this section, therefore, we perform resonant frequency analysis.

If we consider only the mass-spring system, the dynamic equation of the system is given as

$$\left[I_{uu}^{*}\right]\ddot{u}+\left[K_{uu}\right]u=R\,. \tag{41}$$

The natural frequency is obtained as

$$[\omega_{uu}][\omega_{uu}]^{T}=\left[I_{uu}^{*}\right]^{-1}\left[K_{uu}\right], \tag{42}$$

where $u$ is the output vector composed of displacements of the end-point in the direction of x, y, and z, with respect to the global coordinates. $\left[I_{uu}^{*}\right]$ and $\left[K_{uu}\right]$ are obtained by Eq. (43) and Eq. (44), respectively.

$$\left[I_{uu}^{*}\right]=\sum_{i=1}^{3}\left\{\left[{}_{i}G_{u}^{\phi}\right]^{T}\left[{}_{i}I_{\phi\phi}^{*}\right]\left[{}_{i}G_{u}^{\phi}\right]\right\} \tag{43}$$

and

$$\left[K_{uu}\right]=\sum_{i=1}^{3}\left\{\left[{}_{i}G_{u}^{\phi}\right]^{T}\left[{}_{i}K_{\phi\phi}\right]\left[{}_{i}G_{u}^{\phi}\right]\right\}, \tag{44}$$

where $\left[{}_{i}I_{\phi\phi}^{*}\right]$ is a $3\times3$ joint referenced effective inertia matrix of the i[th] serial chain[6]. $\left[{}_{i}G_{u}^{\phi}\right]$ is the inverse matrix of the Jacobian of the i[th] serial chain. And, the stiffness matrix of the i[th] serial chain, $\left[{}_{i}K_{\phi\phi}\right]$, is represented as

$$\left[{}_{i}K_{\phi\phi}\right]=diag\left[{}_{i}k_1,\ {}_{i}k_2,\ {}_{i}k_3,\ {}_{i}k_4,\ {}_{i}k_5\right], \tag{45}$$

where ${}_{i}k_j$ is the stiffness of the j[th] joint in the i[th] serial chain. The structure of the mechanism is made of S45CM. The values of joint stiffnesses are obtained based on an analytic model proposed by [8] and [9].

Now, we can calculate the resonant frequency of the proposed micromanipulator using SVD (Singular Value Decomposition). When the matrix A is defined as

$$\begin{aligned}A&\triangleq[\omega_{uu}][\omega_{uu}]^{T}\\&=U\Sigma V^{T}\end{aligned}, \tag{50}$$

the i[th] singular value $\sigma_i$ of the diagonal matrix $\Sigma$ is obtained as

$$\sigma_i=U_i^{T}AV_i\,, \tag{51}$$

where $U$ and $V$ are orthogonal matrices with respect to the input and the output vector, respectively. So, the resonant frequency, $f_i$, is given as

$$f_i=\frac{\sigma_i}{2\pi}\,. \tag{52}$$

Calculated frequencies are represented in Table 5. Accordingly, control frequency band must be decided based on the least value, $f_1$, not to excite vibration.

Table 5. Calculated natural frequencies of the proposed manipulator

| | $f_1$ | $f_2$ | $f_3$ |
|---|---|---|---|
| Value(Hz) | 174 | 582 | 565 |

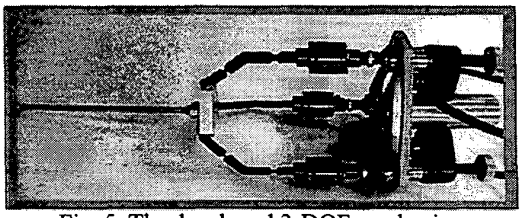

Fig. 5. The developed 3-DOF mechanism

Based on the analytic results, the proposed mechanism is developed as shown in Fig. 5. Fig. 6 (a) shows the feature of the manipulation system. The system consists of coarse and fine dual-stages, a microscope, a micro-gripping mechanism, and master device. The micro-gripping mechanism, which is made up of tungsten-wires, piezoelectric bimorph benders, and force sensors, is attached at the top platform of the micromanipulator.

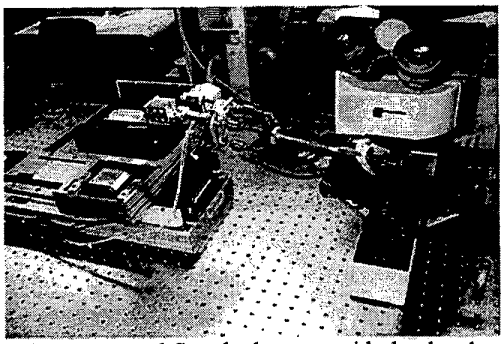

(a) The coarse and fine dual-stages with the developed 3-DOF micromanipulator and microscope

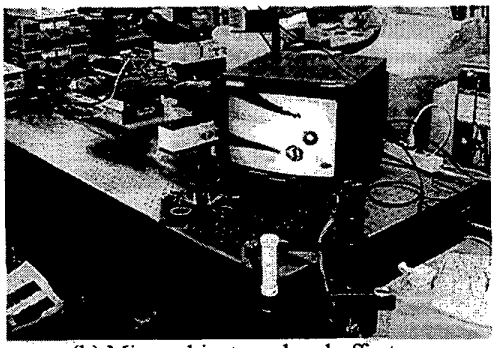

(b) Micro objects and end-effectors

Fig. 8. Tele-micromanipulation system

Specially, an extremely sensitive force sensor based on MEMS technology has been fabricated to deal with force reflection when the micro-gripper grasps a particle in the order of several micron-meters. The positioning accuracy of the proposed tele-micromanipulator is about $1\ \mu m$. Fig. 7 (b) displays the window showing that the micro-gripper attached to the 3-DOF mechanism is approaching to an aluminum bead of $20\ \mu m$.

## 6. Conclusion

We proposed a design methodology for a 3-DOF micromanipulator. Based on preliminary kinematic analysis including inverse and internal kinematics, the relation between the input vector and the effective stiffness model of the system is derived. This relation is employed in actuator sizing for a specified workspace. Furthermore, FEM analysis and resonant frequency analysis are performed to validate the results of analytic study. The designed device was successfully implemented to tele-micromanipulation system having positioning accuracy of $1\ \mu m$.

Our future work will be applications of the developed 3-DOF tele-micromanipulator to manipulation of bio-cells. Also, study on hybrid-type chopstick mechanism made of 6-DOF module plus 3-DOF module is under progressing to deal with more dexterous manipulation of micro-objects. Furthermore, design of a dual-haptic master device is under study.

## References


[1] M. Sitti and H. Hashimoto, "Tele-Nanorobotics Using Atomic Force Microscope", in Proc. IEEE/RSJ Int. Conf. on Intelligent Robots and Systems, Victoria, B.C., Canada, October, pp. 1736-1746, 1998.

[2] T. Tanikawa, T. Arai and T. Masuda, "Development of Micro Manipulation System with Two-Finger Micro Hand". in Proc. IEEE/RSJ Int. Conf. on Intelligent Robots and Systems, Osaka, Japan, Nov. 4-8, pp. 850-855, 1996.

[3] K. M. Lee and D. K. Shah, "Kinematic Analysis of a Three Degrees of Freedom In-Parallel Actuated Manipulator", in Proc. IEEE Int. Conf. on Robotics and Automation, pp. 345-350, 1987. Also in IEEE Journal of Robotics and Automation, Vol.4-3, pp.354-360, 1988.

[4] Y. Ohya, T. Arai, T. Tanikawa, et al., "Development of 3-DOF Finger Module for Micro Manipulation". in Proc. IEEE/RSJ Int. Conf. on Intelligent Robots and Systems, Kyongju, Korea, October. 17-21, pp. 894-899, 1999.

[5] J. Nielsen, T. Tanikawa and T. Arai, "Design and Analysis of a 3-DOF Micromanipulator, " in Proc. IEEE Int. Conf. on Robotics and Automation, Detroit, Michigan, pp. 2183-2188, 1999.

[6] Freeman, R.A. and Tesar, D., "Dynamic modeling of serial and parallel mechanisms/robotic systems, Part I-Methodology, Part II-Applications," Proc. of 20th ASME Mechanisms Conference, Orlando, FL, 1988.

[7] J. Craig, Introduction to Robotics, Addison-Wesley, Menlo Park, CA., 1986.

[8] J. M. Paros and L. Weisbord, "How to design flexure hinge," Machine Design, Vol. 37, No. 27, pp. 151-157, 1965.

[9] J.W. Ryu, "6-Axis Ultraprecision Positioning Mechanism Design and Positioning Control", Ph. D. Dissertation, Department of Mechanical Engineering, Korea Advanced Institute of Science and Technology, 1997.